Available online at www.sciencedirect.com
SCIENCE DIRECT®
Journal of Solid State Chemistry 177 (2004) 4368–4371
JOURNAL OF SOLID STATE CHEMISTRY
http://elsevier.com/locate/jssc

Rapid Communication

In situ formation of Ni nanoparticles supported on $NiFe_2O_4$ by calcination

Fengxi Chen,[a,*] Ziyi Zhong,[a] Xiao-Jun Xu,[b] and Yuxiang Chen[c]

[a] *Department of Appalied Catalysis, Institute of Chemical and Engineering Sciences, 1 Pesek Road, Jurong Island 627833, Singapore*
[b] *Department of Materials Science and Engineering, University of Pennsylvania, 3231 Walnut, Street, Philadelphia, PA 19104, USA*
[c] *Southwest Petroleum Institute, No.8 Xindu Road, Xindu District, Chengdu 610500, China*

Received 27 April 2004; received in revised form 26 May 2004; accepted 28 May 2004

Abstract

$Ni/NiFe_2O_4$ composites have been successfully prepared by calcination at 400°C in air of the mixture $K_3[Fe(ox)_3]\cdot 2.5H_2O$ and $NiCl_2\cdot 6H_2O$ with a molar ratio of 0.7–2. The products are featured by the Ni crystallite size of 15–34 nm, BET surface area of 23–41 m^2/g and variable Ni loadings. TGA and FTIR results indicate in situ generation of CO molecules from decomposition of $K_3[Fe(ox)_3]\cdot 2.5H_2O$. These in situ generated CO molecules account for the formation of Ni nanoparticles by reduction of Ni(II) ions.

Keywords: Supported Ni catalysts; Ferrites; Precursor; TG-FTIR; Thermal decomposition

1. Introduction

CO_2 decomposition is an important reaction to mitigate the global greenhouse effects for environmental protection. It has been demonstrated that Ni, Zn, Co, Cu, etc. bearing oxygen deficient ferrites (ODF) are highly efficient to decompose CO_2 to carbon and oxygen with little or no CO as a by-product [1–4]. It was also reported that the mixed phase comprising a metallic phase (e.g., α-Fe) and oxygen deficient Ni(II)-bearing ferrites (ODNF) had a much higher reactivity toward CO_2 decomposition than the single ODNF phase [5]. The α-Fe was formed while reducing the Ni(II)-bearing ferrites ($NiFe_2O_4$, NF) in the H_2 atmosphere at 300°C. The higher activity of the mixed phase was assigned to the scouting effects of the metallic phase prior to the reaction between CO_2 and ODNF [5].

Ni-loading NFs are desirable. Ni nanoparticles may participate in all three sequences of the CO_2 decomposition: H_2 reduction to generate ODF, CO_2 decomposition on ODF, and re-generation of used ferrites by H_2 (or methanation) [2]. As in the case of α-Fe/ODNFs [5], the Ni nanoparticles can also be expected to show the scouting effects before ODNF reacts with CO_2. Particularly, the generation and re-generation of ODF by H_2 can be promoted by supporting fine nickel particles via hydrogen spillover mechanism. This phenomenon has already been observed in previous studies of the redox behaviors of ZrO_2 or its mixed metal oxide solid solutions (e.g., CeO_2–ZrO_2) with the supported Ni/NiO nanoparticles [6,7].

The objective of the present study is to prepare such supported catalysts (i.e., Ni/NFs) by calcination. In contrast to the previous methods [4,5], which consist of two consecutive steps (i.e., preparation of NFs followed by H_2 reducing), the calcination method can be carried out in ambient atmosphere, and the metallic and spinel phases are directly formed.

2. Experimental

2.1. Preparation

All reagents ($FeCl_3\cdot 6H_2O$, $K_2C_2O_4\cdot H_2O$ and $NiCl_2\cdot 6H_2O$) are A.R. grade from Aldrich, and used as received. Potassium iron (III) oxalate (PIO,

*Corresponding author. Fax: +65-6316-6182.
E-mail address: chen_fengxi@ices.a-star.edu.sg (F. Chen).

0022-4596/$ - see front matter © 2004 Elsevier Inc. All rights reserved.
doi:10.1016/j.jssc.2004.05.052

$K_3[Fe(ox)_3] \cdot 2.5H_2O$)[1] and $NiCl_2 \cdot 6H_2O$ are used as iron and nickel sources, respectively. A typical procedure is given as follows: PIO was mixed with $NiCl_2 \cdot 6H_2O$ at the molar ratio, M_r, of PIO to Ni(II) of 0.7–2. The mixture was ground in a ceramic mortar to get a dough-like precursor, followed by calcination in a 400°C muffle furnace for 2.5 h. After naturally cooling down to room temperature (r.t.), the resulting powder was dispersed into distilled water with the solid to liquid ratio of 1 g/40 mL, and stirred at 80°C hot plate and 600 rpm for 1 h to remove the excess salts (e.g., unreacted starting materials). The final products were recovered by filtration, and dried under ambient conditions for subsequent characterizations.

2.2. Characterizations

The phases present in the products were identified from their powder X-ray diffraction (PXRD) patterns, which were collected on Siemens D5005 with Cu$K\alpha$ radiation ($\lambda = 1.5406$ Å) operated at 40 mA and 40 kV. The crystalline size was calculated using Scherrer equation, $D_{h\,k\,l} = 0.9/B_{h\,k\,l} \cos\theta$, where $D_{h\,k\,l}$ is the crystallite size, λ is the incidence wavelength of X-ray radiation, $B_{h\,k\,l}$ is full-width at half-height of the peak, and θ is the corresponding diffraction angle.

Thermal Analysis was conducted on Universal V2.5H TA Instruments (Model: SDT 2960) in N_2 (purity: 99.9995% from Soxal, flow rate: 90 mL/min). The thermogravimetry was connected with 70 cm stainless steel tube to Bio-Rad FTIR spectrophotometer (Model: Excalibur series, FTS 35000ARX), which allows for the direct detection of the decomposition products during TGA. Before starting thermal analysis, the system was flushed with N_2. The temperature was dwelled at 100°C for 0.5 h and then increased to 1000°C with the heating rate of 10°C/min. Thermal degradation profiles (i.e., TGA curves) and their first derivatives (differential thermogravimetric analysis, DTG curves) were recorded to determine the weight loss over a certain temperature range and their corresponding peak position.

Adsorption isotherms were measured using nitrogen gas as the adsorbate on Quantachrome Autosorb-6 at 77 K. Before measurement, the sample was outgassed at 300°C for 21 h. The BET surface area was calculated using the BET equation in the range of relative pressures between 0.04 and 0.4.

3. Results and discussion

When the procedure described in Section 2.1 is followed, Ni/NFs composites are prepared. Their PXRD patterns are shown in Figs. 1b–e. Besides those strong peaks attributable to the NF spinel phase [JCPDS 86-2267], three extra peaks, indicated by asterisks in Fig. 1b, were observed at $2\theta = 44.5°$, 51.8° and 76.4°. They can be respectively indexed to the (111), (200) and (220) reflections of the Ni(cubic) phase [JCPDS 87-0712]. The Ni crystallite size was estimated from its (111) peak to be in the range of 15–34 nm. The BET surface area, $S_{BET,}$ varies between 23 and 41 m^2/g. According to the results shown in Table 1, a Ni/NFs nanocomposite with S_{BET} of 41 m^2/g and the highest loading (see Discussion below) of fine Ni particles (ca. 15 nm) can be formed under optimal conditions (i.e., $M_r = 2$, 400°C, 2.5 h).

The relative peak intensities at $2\theta = 35.8°$, 43.4° and 63.0° are obviously intensified than those of the single NF spinel phase, implying the co-existence of NiO(cubic) [JCPDS 78-0429] in the products. The NiO(cubic) phase, from which hydrogen has also been observed to spill over into CeO_2–ZrO_2 supports [6], may result from thermal decomposition of the Ni(II) salt, or partial oxidation of the earlier formed metallic Ni particles in ambient atmosphere. The measured XRD curves cannot be well fitted with any combination of the spinel and NiO phases with different weight ratios, suggesting that other factors such as the distorted spinel lattice may also contribute to the XRD profiles. In this case, the relative peak intensity of $2\theta = 63.0°$ (existing in both the spinel and NiO phases) to $2\theta = 35.8°$ (unique in the spinel phase), $I_{63/35.8,}$ was taken to qualitatively describe the NiO content in the mixed phases. Similarly, $I_{44.5/35.8}$ was used to qualitatively describe the Ni content supported on the NFs.

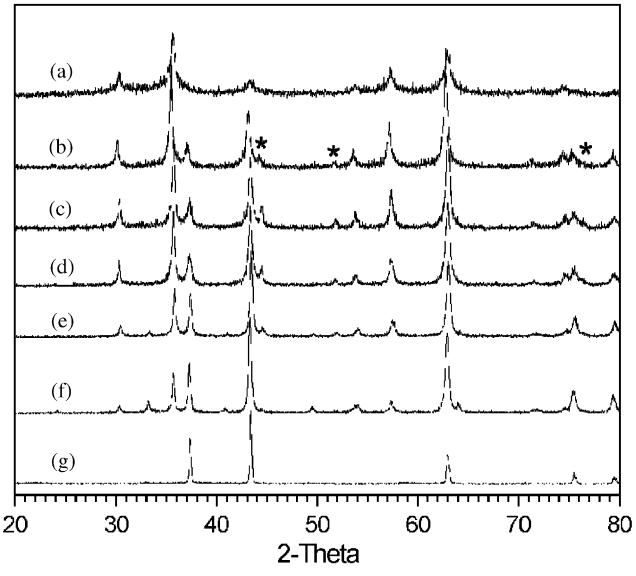

Fig. 1. Powder XRD patterns of the products prepared under different molar ratios of PIO to Ni(II). (a) ∞; (b) 2.0; (c) 1.3; (d) 1; (e) 0.7; (f) 0.5, and (g) 0. Asterisks in curve *b* indicate the peaks due to the presence of the Ni(cubic) phase.

[1] Potassium iron (III) oxalate (PIO, $K_3[Fe(ox)_3] \cdot xH_2O$, x is between 2.5 and 3 depending on the extent of dryness) was prepared by the standard method and purified by repeated re-crystallization. For more details, see Ref. [8].

Table 1
Influence of the molar ratio of PIO to Ni(II) on phase composition of the product[a]

Molar ratio, M_r	∞	2	1.3	1	0.7	0.5	0
Phase composition	Fe_3O_4	$NiFe_2O_4$ NiO Ni	$NiFe_2O_4$ NiO Ni	$NiFe_2O_4$ NiO Ni	$NiFe_2O_4$ NiO α-Fe_2O_3 Ni	$NiFe_2O_4$ NiO α-Fe_2O_3	NiO
Crystallite size of Ni (nm)	—	15	30	33	34	—	—
$I_{63/35.8}$	0.77	1.48	1.66	2.07	2.63	2.80	—
$I_{44.5/35.8}$	—	0.17	0.19	0.14	0.10	—	—
S_{BET} (m^2/g)	61	41	31	35	23	14	35

[a] Reaction parameters: 400°C, static air, 2.5 h.

Table 2
Influence of temperature on phase composition of the product[a]

Temperature (°C)	300	400	500	600	700	800
Phase composition	$NiFe_2O_4$ NiO	$NiFe_2O_4$ NiO Ni	$NiFe_2O_4$ NiO	$NiFe_2O_4$ NiO	$NiFe_2O_4$ NiO	Fe(Ni)O
$I_{63/35.8}$	1.22	1.48	1.67	1.74	3.76	∞

[a] Reaction parameters: molar ratio of PIO to Ni(II) of 2, static air, 2.5 h.

The value of M_r and the calcination temperature affect the phase composition of the product. At 400°C, magnetite (Fe_3O_4, JCPDS 88-0866) or maghemite (γ-Fe_2O_3, JCPDS 25-1402) is formed from pure PIO. With the addition of Ni(II), three features can be found from Table 1. Firstly, $I_{63/35.8}$ gradually increases with the decrease of M_r, implying the increase of NiO content. Secondly, the metallic Ni phase appears with almost constant content ($I_{44.5/35.8}$: ca. 0.20) when M_r is 1.3–2. However, its crystallite size increases from 15 to 34 nm with the Ni(II) addition. Lastly, the metallic Ni phase gradually disappears with more Ni(II) addition (i.e., $M_r < 0.7$). Instead, some new peaks (e.g., 2θ 33.2°) occur indicating the formation of α-Fe_2O_3 [hematite, JCPDS 87-1166]. At the fixed M_r of 2, Ni nanoparticles are formed only at 400°C. The NiO formation is promoted with increasing the calcination temperature, as shown by the increase of the $I_{63/35.8}$ value in Table 2. A FeO–NiO solid solution is formed above 800°C.

Thermal analysis results of $K_3[Fe(ox)_3] \cdot 2.5H_2O$ in Fig. 2 and Table 3 shed some insight into mechanistic aspects about the in situ formation of the Ni nanoparticles. TGA curve in Fig. 2 includes PIO dehydration before 100°C and decomposition of anhydrous PIO later on. During dehydration, 2.5-coordinated water molecules (ca. 9.2 wt%) are evolved. Two steps are involved at early stages of decomposition of anhydrous PIO: evolution of the CO molecules between 292°C and 455°C and then the mixture of CO and CO_2 between 550°C and 780°C. Weight loss above 800°C indicates further pyrolysis of the K–Fe–C–O residues.

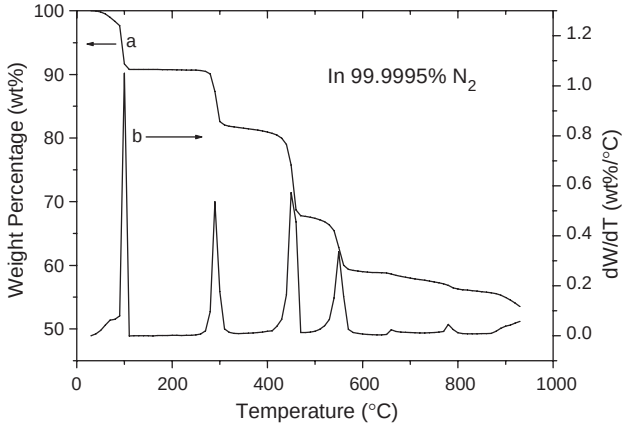

Fig. 2. Thermal analysis results of PIO in N_2. (a) TGA curve and (b) DTG curve.

Table 3
TGA results of PIO in 99.9995% N_2

Peak position (°C)		76	98	292	455	550	780
Weight loss (wt%)	Experimental	76	98	9.7	13.7	8.4	2.9
	Calculated	9.2		23.2		11.2	
	Assignment	2.5 H_2O		4CO		3/4 ($CO + CO_2$)	

Some evidences can be found from in situ FTIR spectra (Fig. 3) supporting the generation of the CO and CO_2 molecules during PIO decomposition in N_2. Two peaks at 2324 and 2358 cm^{-1} in Figs. 3b and c are due to

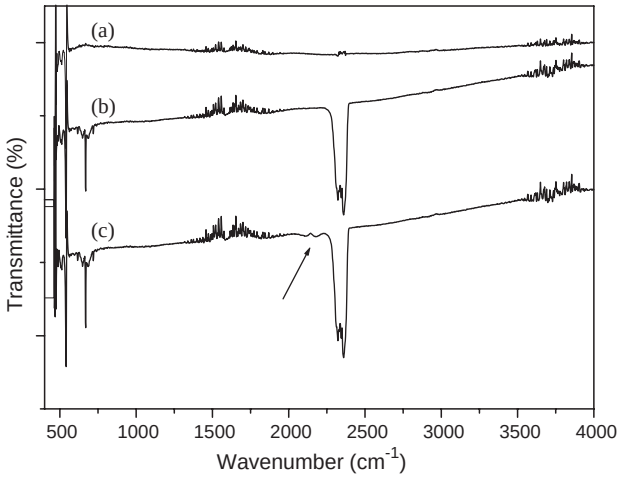

Fig. 3. FTIR spectra of decomposition products from TGA analyses in N_2. (a) 100–150°C, (b) 220–320°C and (c) 370–470°C. The peak marked by an arrow in curve *c* is due to the presence of CO.

the presence of CO_2 in the decomposition products. A small peak at ca. 2200 cm^{-1} in Fig. 3c indicates the presence of CO [9,10]. The "negative" transmittance in the range of the water band for all curves in Fig. 3 indicates that the recorded amount of water is smaller than in background spectrum. It should be related to incomplete flushing of the TGA-FTIR system before the collection of the background spectrum, or condensation of the water product in the duct where it is carried from TGA chamber to FTIR. (Note: relative humidity in Singapore is quite high, usually 70–90%.) The lack of the CO signal between 220°C and 320°C in Fig. 3b may be related to the O_2 impurity in the background water [11].

It is understandable that Ni nanoparticles are formed from reduction of Ni(II) ions with in situ generated CO as a reducing agent [12]. It is noteworthy that using the multinuclear Ni–Fe bimetallic complex (e.g., $Ni_3Fe_6O_4(C_6H_6O_7)_8 \cdot H_2O$) [13] as the single molecular precursor under similar conditions, no metallic phase could be observed except the mixed $NiFe_2O_4$ and NiO phases, although the CO formation was also suggested during thermal decomposition of the organic components.

The principle of this work should be applicable to a wide range of metallic phases (e.g., Fe, Co, Cu, Cd, Zn, etc.) supported on the spinel phases; providing the decomposition rate of the organic components and the reducing rate of the targeted metal ions are delicately balanced in kinetics.

4. Conclusions

Starting from iron(III) oxalate complex and Ni(II) salt, the Ni/NFs nanocomposites are successfully prepared with Ni crystallite size of 15–34 nm, S_{BET} of 23–41 m^2/g and various Ni loadings by calcination at 400°C in ambient atmosphere. Thermal analyses show that the in situ generated CO molecules from the decomposition of the oxalate ligands are responsible for the formation of metallic Ni phase.

Acknowledgments

FX Chen acknowledges the financial support by ICES in-house project (project code: ICES/03-112002).

References

[1] Y. Tamaura, M. Tabata, Nature 364 (1990) 255.
[2] S. Komarneni, M. Tsuji, Y. Wada, Y. Tamaura, J. Mater. Chem. 7 (1997) 2339.
[3] J.-S. Kim, J.-R. Aha, J. Mater. Sci. 36 (2001) 4813.
[4] H.-C. Shin, S.-C. Choi, K.-D. Jung, S.-H. Han, Chem. Mater. 13 (2001) 1238.
[5] M. Tsuji, Y. Wada, T. Yamamoto, T. Sano, Y. Tamaura, J. Mater. Sci. Lett. 15 (1996) 156.
[6] T. Takeguchi, S.-N. Furukawa, M. Inoue, J. Catal. 202 (2001) 14.
[7] H.-S. Roh, W.-S. Dong, K.-W. Jun, S.-E. Park, Chem. Lett. (2001) 88.
[8] H.S. Booth (Ed.), Inorganic Syntheses, Vol. 1, McGraw-Hill, New York, 1939, p. 36.
[9] M. Guillot, M. Richard-Plouet, S. Vilminot, J. Mater. Chem. 12 (2002) 851.
[10] W. Stichert, F. Schüth, S. Kuba, H. Knözinger, J. Catal. 198 (2001) 277.
[11] S.L.Soled Iglesia, G.M. Kramer, J. Catal. 144 (1993) 238.
[12] E.R. Leite, N.L.V. Carreño, E. Longo, A. Valentini, L.F.D. Probst, J. Nanosci. Nanotech. 2 (2002) 89.
[13] N.S. Gajbhiye, S. Prasad, Thermochim. Acta 285 (1996) 325.